SAND2000-0143J

Spectral resolution for five-element, filtered, x-ray detector (XRD) arrays using the method of Backus and Gilbert.

D. L. Fehl, F. Biggs, G. A. Chandler, and W. A. Stygar
Sandia National Laboratories
Albuquerque, New Mexico
(505) 845-7822

ABSTRACT

The generalized method of Backus and Gilbert (BG) is described and applied to the inverse problem of obtaining spectra from a 5-channel, filtered array of x-ray detectors (XRD's). This diagnostic is routinely fielded on the Z facility at Sandia National Laboratories to study soft x-ray photons ($\leq$ 2300 eV), emitted by high density Z-pinch plasmas. The BG method defines spectral resolution limits on the system of response functions that are in good agreement with the unfold method currently in use. The resolution so defined is independent of the source spectrum. For noise-free, simulated data the BG approximating function is also in reasonable agreement with the source spectrum (150 eV black- body) and the unfold. This function may be used as an initial trial function for iterative methods or a regularization model.

I. Introduction

Arrays of individually filtered detectors have been used to study x-ray spectra since the time of Röntgen and Barkla[1]. This technique consists of simultaneously exposing several detectors of differing spectral response to x rays and inferring information about the incident spectrum from the data. The method is often capable of yielding coarse spectral estimates and is also useful in testing theoretically-derived spectra. While now largely supplanted by energy- and wavelength-dispersive methods to study steady-state x-ray sources, it is however still used to diagnose x rays emitted by high temperature, pulsed plasmas[2]. In particular, for investigating the spectra of soft x rays emitted by laser-driven and Z-pinch plasmas, filtered-detector arrays have been made of thin-film K- and L-edge filters coupled to photoemissive x-ray detectors (XRDs)[3], XRDs plus mirrors[4], silicon PIN detectors[5], monolithic silicon photodiodes[6], photoconductive detectors[7], and microchannel plates[8].

An array of five, time-resolved, filtered XRDs[9] is used at the Z-facility[10] (a 20 MA, Z-pinched plasma source) to measure x-ray flux and fluence. (Other applicable x-ray diagnostics include bolometers[11], calorimeters[12], and a transmission grating spectrometer[13].) Typical response functions for such an array are shown in Fig. 1. These overlapping functions are characterized by sharp, x-ray edge features as well as by a "hump" at higher photon energies. Representative signals are shown in Fig. 2. When the detectors are run in a linear current regime, the time-dependent XRD data $g_i(t)$ (i = 1,2, ..., 5) may be described by a system of Fredholm integral equations (first kind):

$$g_i(t) = \int_0^\infty f(E,t) R_i(E) dE + \epsilon_i(t) \qquad (1),$$

where f is the unknown source spectrum (differential flux), R_i is the i-th response function, E is the x-ray photon energy, and t is the time. The random variable ϵ_i represents noise. The integral limits in Eqs. (1) reflect the largest possible energy domain for f; in practice, this domain may be reduced to the finite interval $[E_{min},E_{max}]$ and the interval limits adjusted, depending on the relative shapes of the incident spectrum and the response functions. (See Appendix I.) To obtain the spectrally-integrated x-ray flux incident on the XRD array, one estimates f from Eqs. (1) and computes $\int f(E,t)dE$. The x-ray fluence is then the time integral of the flux.

The estimation of a source f from a set of response functions and discrete data, as in Eqs. (1), is a well-known, non-trivial, linear inversion problem[14-21]. A complete pointwise reconstruction (or unfold) of f is not possible generally due to non-uniqueness: *i.e.,* to any unfolded solution one can add an infinite number of (usually highly oscillatory) functions that average out to zero in Eqs. (1). Numerical instabilities are also common. But, the existence of such difficulties does not preclude the recovery of useful information about f – if the possible number of solutions can be limited and oscillations controlled. To guide the unfolding process, most classical and modern inversion techniques rely on some inclusion of relevant information about the measurement or source *in addition* to the data and responses (*e.g.,* known spectral values, functional parametrizations, regularization,[14-21] interpolation constraints).

A first step in deciding what information to add is taken by understanding the averaging behavior of the coupled system of Eqs. (1). The *system* of responses (as opposed to individual response functions) defines the scale and location of source detail retained by the data and thus defines the spectral resolution of the measurement. Armed with an estimate of resolution, one may suggest constraints for the unfold. For example, one may suggest how to partition the spectral domain for a simple histogram-type solution of Eqs. (1) or judge whether emerging details in a more complicated unfold are likely to be present in the source spectrum.

A little-used technique for studying inverse problems as posed by Eqs. (1) was introduced by Backus and Gilbert (BG)[22-24]. Their procedure attempts to modify the given response functions R_i into more localized responses. The narrowest of these characterize the ability of Eqs. (1) to resolve spectra, independent of the source f. The method also defines an *estimate* f_{BG} of f at each photon energy of interest.

This paper describes the application of the Backus-Gilbert method to the inverse problem posed by XRD arrays at the Z-facility. The issue is what information this method can give to an unfold procedure. The BG method for constructing an averaging kernel from a

DISCLAIMER

DISCLAIMER

Portions of this document may be illegible in electronic image products. Images are produced from the best available original document.

set of response functions is described in Sect. II The results of a BG analysis applied to the XRD array for simulated *noise-free* data are given in Sect. III and compared in Sect. IV to the unfold analysis currently in use at the Z facility. Details of the unfold procedure are given in Appendix I. The notion of an averaging kernel, inherent to the BG method and rarely considered in the x-ray diagnostics literature, is discussed in Appendix II.

II. The Backus-Gilbert method

Central to the Backus-Gilbert approach is the realization that one not need deal with Eqs. (1) as written. Rather, without distorting the problem, one can form linear combinations of the equations. Such simultaneous manipulations (transformations) of both data and integrals may advantageously modify the integrands and thus yield a more manageable inversion problem. This basic insight is illustrated in Fig. 3. Shown in Fig. 3a are three, hypothetical response functions $\{R_1, R_2, R_3\}$, two of which overlap. Assume that these responses belong to a three-element detector array that produces corresponding noise-free data $\{g_1, g_2, g_3\}$ from some unknown spectrum f according to Eqs. (1). One wishes to estimate f incident on this instrument within the domain $[E_{min} = E_1 - \Delta E,\ E_{max} = E_5 + \Delta E]$, defined here by the response functions. The basic BG analysis has two parts. First, it is clear that a narrower, transformed set of response functions can be obtained (Fig. 3b) if one combines the last two responses: *i.e.*, define $R_3' \equiv R_3 - (h_3/h_2)R_2$. The set $\{R_1, R_2, R_3'\}$ has now three *non*-overlapping responses. One may argue that $\{R_1, R_2, R_3'\}$ determines the smallest details in f that can be obtained by *this particular* instrument[25]. The second step in the BG analysis estimates the source function. If one forms the *same* linear combination of the original data as for the transformed responses, one generates *transformed* data $\{g_1, g_2, g_3' \equiv g_3 - (h_3/h_2)g_2\}$. For this simple case, dividing each transformed datum by the width of its transformed response, one estimates source function values $g_1(2h_1\Delta E)^{-1}$, $g_2(2h_2\Delta E)^{-1}$, and $g_3'(2h_3\Delta E)^{-1}$, which turn out to be simple averages of the source over the narrower bins centered at E_1, E_3, and E_5, respectively. The full BG technique differs from this illustration in providing a general method for choosing the linear combination of responses and in estimating f at arbitrary photon energies within the domain $[E_{min}, E_{max}]$.

The Backus-Gilbert technique starts with the set of response functions $\{R_i(E)\}_{i=1}^{N}$, where N is the number of filtered detectors, or channels. For each photon point of interest E_0 at which one wishes to estimate f, the method finds the linear combination of response functions that is as narrow as possible according to prescribed criteria. Thus define

$$A_{BG}(E_0,E) = \sum_{i=1}^{N} \alpha_i(E_0) R_i(E) \qquad (2).$$

on the practical domain $[E_{min}, E_{max}]$. As shall be clear presently, A_{BG} may be called an averaging kernel (AK), a scanning function[20], or a sampling function; A_{BG} depends on the photon energy E but is different for each point of interest E_0. The scalars $\{\alpha_i\}$, which may be positive, negative or zero, are then chosen to make

$$\int_{E_{min}}^{E_{max}} (E_0 - E)^2 A_{BG}(E_0,E)^2 dE = \textit{minimum} \quad (3),$$

and

$$\int_{E_{min}}^{E_{max}} A_{BG}(E_0,E)\, dE = 1 \qquad (4),$$

for fixed E_0. In Eq. (3) the arbitrary weighting term $(E_0 - E)^2$ and square of the AK accentuate a narrow result. The minimization procedure to obtain the α_i's uses the method of Lagrange multipliers and is well described in the literature[14-16,23]; the resulting matrix procedure has been programmed in FORTRAN[26].

Backus and Gilbert also define two mathematical diagnostics for characterizing $A_{BG}(E_0, E)$. Reminiscent of the "mean" and "variance" from probability theory, both measures are functionals of the AK shape as well as functions of E_0. The "center" $c[A_{BG}]$ of A_{BG} is defined as

$$c[A_{BG}] = \frac{\int_{E_{min}}^{E_{max}} E\, A_{BG}(E_0,E)^2 dE}{\int_{E_{min}}^{E_{max}} A_{BG}(E_0,E)^2 dE} \qquad (5).$$

the "width" $w[A_{BG};E_0]$ of A_{BG} is defined as

$$w[A_{BG}] = 12 \int_{E_{min}}^{E_{max}} (E - c[A_{BG}])^2 A_{BG}(E_0,E)^2 dE \qquad (6).$$

The center diagnostic c thus defines a weighted average energy for the AK A_{BG} (at fixed E_0),

and the width[27] w is a measure of the spread A_{BG} about its center. One notes the same use of A_{BG}^2 in Eqs. (5) and (6) as in (3).

If the AK $A_{BG}(E_0, E)$, derived from Eqs. (3) and (4), is taken as a transformed (possibly improved) response function for the experiment, then the integral of the source f with A_{BG} by Eqs. (1) produces transformed data in the spirit of Fig. 3. Backus and Gilbert define the function f_{BG}:

$$f_{BG}(E_0) \equiv \int_{E_{min}}^{E_{max}} A_{BG}(E_0,E) f(E)\,dE = \sum_{i=1}^{N} \alpha_i(E_0) \int_{E_{min}}^{E_{max}} R_i(E) f(E)\,dE = \sum_{i=1}^{N} \alpha_i(E_0) g_i \approx f(E_0) \quad (7).$$

This definition justifies the use of synonymous terms like *averaging kernel, scanning function,* and *sampling function* for A_{BG}, used above, since for each selected E_0 A_{BG} averages, scans, or samples f over the x-ray energies to which the instrument (represented by the R_i's) responds. The transformed result of such an interaction is the original data g_i, weighted by the *same, known* scalars $\{\alpha_i\}$ that determine $A_{BG}(E_0, E)$. That $f_{BG}(E_0)$ should also *approximate* $f(E_0)$ in Eq. (7) is due to two considerations: (1) the normalization constraint on A_{BG} [Eq. (4)] makes the scalars $\{\alpha_i\}$ inversely proportional collectively to the set of integrals $\int R_i(E)dE$ (the calibration information)[28]; and (2) the narrower the width of A_{BG} and the closer its center to E_0, the more local is the average of f with A_{BG}. (Appendix II gives an heuristic argument for the constraints Eqs (3) and (4) and describes other properties of AKs that relate to the BG method.)

In the BG formulation the notion of spectral resolution also arises from Eq. (7). That is, f_{BG} results because A_{BG} effectively samples the unknown source f over a finite subregion of the domain. Roughly speaking, details in f on a finer scale than the width of A_{BG} at E_0 will average out in Eq. (7) or be weakly reproduced in f_{BG}. It is reasonable, therefore, to associate the width $w[A_{BG}]$ with each estimate $f_{BG}(E_0)$ as a pointwise measure of resolution or resolving power. One can also assign resolution bands to the whole photon energy domain by selecting a finite subset of the AK's that together span it. (See Sect. IV.) In either sense *resolution* refers to no particular source function.

III. Test problem and results

We have applied the BG method to the response functions of the 5-channel, filtered-XRD diagnostic, described above. Following Eqs. (1) we folded an arbitrary 150 eV blackbody spectrum (Fig. 4) with the response functions R_i (Fig. 1) to obtain the noise-free,

fixed-time data g_i, shown in the lower curve of Fig. 5. The Backus-Gilbert AK A_{BG} was constructed at several observational points E_0, together with the center and width diagnostic functions and the f_{BG} approximation. For these calculations, the spectral domain $[E_{min}, E_{max}]$ was defined as [137, 2300] eV and the simulated data unfolded by the methods summarized in Appendix I.

Figure 6 shows the evolution of the averaging kernel A_{BG} with the parameter E_0. This behavior is typical. As E_0 increases, continuously changing contributions α_i from the various response functions [Eq. (2)] give the impression that A_{BG} also moves (scans) unilaterally to higher energies. For example, when $E_0 = 250$ eV, A_{BG} consists primarily of R_1 modified by a negative correction from R_4, which removes the high energy "hump" of R_1. But as E_0 increases to 350 eV, the contribution from R_1 decreases in $A_{BG}(350,E)$ while the contribution from R_2 increases. At $E_0 = 450$ eV, the contribution of R_2 becomes the major component. The process repeats at $E_0 = 600$ eV when the contribution from R_3 begins to appear and R_2 wanes.

In contrast to the smooth evolution of A_{BG}, the BG measures of width and center oscillate as E_0 increases. For example, in Fig. 7 one can see the width $w[A_{BG}]$ pass through five local minima. Likewise, in Fig. 8 the center measure $c[A_{BG}]$ oscillates about E_0. One can show that c and E_0 coincide when the width w passes through a local minimum. The reason for such broadly oscillatory behavior is that the measures w and c are sensitive to the lateral extension of A_{BG}, which expands and contracts discontinuously with E_0 (Fig. 6) even though the components α_i of A_{BG} change smoothly.

Given the set of coefficients $\{\alpha_i\}$ and the set of simulated data $\{g_i\}$, one can construct the associated approximating function $f_{BG}(E_0)$. This function is compared to the simulating 150 eV spectrum in Fig. 4. It is clear that while $f_{BG}(E_0)$ has roughly the same size and shape as f, and even approximates f well at some points, it deviates significantly from f near the peak and exponential tail.

IV. Discussion

Although the continuous construction of f_{BG} shown in Fig. 4 is not the primary focus of this paper, it helps illustrate the concept of resolution in the BG method. As discussed in Appendix II, one can intuitively understand the pointwise behavior of $f_{BG}(E_0)$ relative to $f(E_0)$ in terms of two independent components: the local shape of f (*i.e.*, slope, curvature, *etc.*) and the resolution of A_{BG} associated with the width $w[A_{BG}]$. In Fig. 4 f_{BG} thus wanders about f as a function of E_0 because f varies in shape and A_{BG} in width. Conversely, one expects the best agreement where f changes most gradually and A_{BG} is narrowest.

Now in such a comparison one has little control over the shape of the incident spectrum f; but one can, however, choose to report f_{BG} only for the narrowest available BG averaging kernels. This is done by selecting values E_0 at which $w[A_{BG}]$ is a local minimum. In the filtered-XRD example, these minima occur at E_0= 250, 450, 850, 1200, and 1800 eV (Fig. 7). The corresponding AK's are clearly less spread out than the rest of the BG kernels [*e.g.*, in Fig. 6 compare $A_{BG}(350,E)$ with $A_{BG}(250,E)$ and $A_{BG}(450,E)$]; they are also, for the most part, improvements over the five, original response functions R_i. For example, comparing Fig. 9 with Fig. 1, one sees that the AK's for E_0= 250, 450, 850 eV are respectively narrower than R_1, R_2, and R_3 because the high energy "humps" have been removed. On the other hand, the AK's for E_0= 1200 and 1800 eV are only slightly narrower than R_4 and R_5 .

Figure 10 compares the known spectrum f with a *discrete* representation of f_{BG} (solid points), based only the five narrowest BG AK's of Fig. 9. The indicated horizontal error bars are the corresponding widths, which represent the resolution of the BG reconstruction process at each energy point. The five points shown are the most accurate BG estimates of f (with this set of response functions) because at these energies the BG AK samples the most limited segments of the source. Moreover, since the width $w[A_{BG}]$ is not calculated from f, the collection of horizontal bars can also be interpreted as a set of resolution bands representing the best overall, spectral detail obtainable from the given responses and *any* source function on the spectral domain $[E_{min}, E_{max}]$. Such bands may turn out to be overlapping or non-contiguous; they may even be somewhat ill-defined, depending on the shallowness of the minima of $w[A_{BG}]$ vs. E_0.

The BG estimate of resolution can provide useful guidance to the unfolding of filtered-XRD data. The unfold procedure described more fully in Appendix I attempts to extract information about the source f only sufficiently well to estimate $\int f(E,t)dE$ over the spectral domain. To do this, one assumes f can be approximated by a *histogram* (defined on a *contiguous* partition of the domain) so that details of f within the bins of the partition average out in $\int f(E,t)dE$. The solid line f_{UNFOLD} in Fig. 10 is such an unfold of the simulated data (solid circles) in Fig. 5. Using this method, one obtains reasonable flux estimates from response functions like those in Fig. 1 *and* blackbody-like spectra[9]: 95% of the flux in the spectral domain is recovered for a 150 eV blackbody and 103% for a 250 eV blackbody (not discussed here). But, a major problem in setting up this unfold procedure is determining the number and location of the bin boundaries (or joints) in the histogram: a poorly-chosen partition can predispose the unfold to spurious structure and excessively bias the estimate of flux. In Appendix I, the bin-selection process is based largely on x-ray absorption edges, an identification that is clear at low photon energies but rather arbitrary at energies higher than the edge features. In particular, a joint at ~1500 eV is not supported by an absorption edge feature. Now, the BG resolution bands provide an independent assessment of the partition because these bands are a measure of the source detail preserved by the response functions. Comparing the horizontal BG resolution bars of f_{BG} with the bins of f_{UNFOLD} in Fig. 10, one finds corroboration for the unfold partition — including a boundary at 1400 - 1500 eV. (Exact agreement between the two methods need not be expected since the selection criteria

differ and the BG resolution bands can be non-contiguous.) When the response functions have no easily identifiable absorption features (*e.g.*, arrays of diamond photoconductors[29] filtered with CH material and used for photon energies ≥ 500 eV), the BG resolution bands may be used as an initial guess for an unfold partition.

The BG method has other uses as well. For example, when one is unfolding with more flexible basis functions (*e.g.*, polynomials) and little *a priori* information, the BG resolution bands can suggest if an unfolded feature is too narrow to be resolved and possibly spurious. More information is needed. Likewise, in more sophisticated unfolding techniques f_{BG} may be used as a trial function or a model for regularization. Lastly, Craig and Brown[19] note a role for the BG in experimental design: by examining the resolution bands of a proposed set of response functions, one may decide that some of the responses need adjustment (*e.g.*, filter changes) to optimize the spectral coverage of the array and the subsequent unfold process.

Like most numerical procedures the BG method is not a panacea. It works well for the type of response functions used here, but there are classes of response functions for which this method[20] gives less satisfactory results. Moreover, as one might expect, the matrix manipulation procedures required in the BG method become numerically unstable as the response functions approach linear dependence. Finally, if one is interested in obtaining f_{BG} from real data, error propagation must be considered. Unlike the inaccuracy studied here, the random uncertainty in f_{BG} due to data imprecision or noise is *inversely* related to the width of the AK: *i.e.*, the narrower the AK, the greater the propagated uncertainty. The general Backus Gilbert method not only provides error propagation information about f_{BG}, it can even incorporate specified error bounds in the minimization process that yields an AK, thus effectively trading resolution off against propagated precision. This option is treated in the literature[14-16,22-24] but is beyond the scope of this paper; it too has been programmed in FORTRAN[26].

Appendix I. The standard unfold for the filtered-XRD array at the Z facility

The unfold for the filtered-XRD arrays at the Z facility uses classical matrix inversion techniques[19,30]. It assumes that the incident source spectrum $f(E)$ can at each time step be approximated by a contiguous set of histogram basis functions $B_j(E)$

$$f(E) \approx \sum_{j=1}^{N} f_j B_j(E) \quad (8),$$

defined on the finite domain $[E_{min},E_{max}]$, which is partitioned into N (= 5) bins of widths ΔE_j, j = 1, ..., N. (The domain boundaries E_{min} and E_{max} are described below.) These basis functions are assumed to have unit height over ΔE_j and be zero elsewhere. Other basis functions, like polynomials or even the response functions themselves (the so-called normal solution[14-17]) can also be chosen; but a histogram was selected because an estimate of the spectral integral of the source function (the flux) is principally sought, not details of the spectrum, and it was desired to automate the unfold with a simple algorithm. By substituting Eq. (8) into Eq. (1) one obtains

$$g_i(t) = \int_0^\infty f(E,t) R_i(E) dE \equiv \sum_{j=1}^{N} f_j \int_{E_{min}}^{E_{max}} R_i(E) B_j(E) dE = \sum_{j=1}^{N} R_{ij} f_j \quad (i = 1,...,N) \qquad (9),$$

where

$$R_{ij} = \int_{E_{j-1}}^{E_j} R_i(E) dE = \Delta E_j \left\langle R_i \right\rangle_j \quad (i,j = 1,...,N) \qquad (10).$$

The elements R_{ij} are thus proportional to the average $\langle R_i \rangle_j$ of the i-th response function in the j-th bin and form an $N \times N$ matrix $\boldsymbol{R}$. If the response functions are linearly independent, the inverse matrix $\boldsymbol{R}^{-1}$ exists — although for response functions like those in Fig. 1 the condition number[14-17,31], which relates to error propagation, is often large (~20 - 30). The unfold-histogram coefficients f_j are then given by

$$f_j = \sum_{j=1}^{N} \left[\boldsymbol{R}^{-1} \right]_{ji} g_i \qquad (11).$$

The inverse matrix is constructed by Singular Value Decomposition[31,32]. A unique solution is obtained by assuming that any other solution to Eq. (1) includes components which solve Eq. (1) with $g_i = 0$ ($\forall$ i = 1, 2, ... , N) and is excluded in Eq. (11)[14-16]. A disadvantage of this formulation is that negative values of f_j can be obtained from noise in real data and also when a histogram is a poor approximation to the source function.

Setting up the spectral domain parameters (E_{min} , E_{max} , and Δ E_j's) of the histogram in Eq. (8) is typically an iterative process that balances successful numerical inversion of $\boldsymbol{R}$ against approximation of the source f. This process is somewhat arbitrary since one must estimate the form of f *a priori*. Yet the choice of histogram parameters is important since ill-placed endpoints and joints may distort the unfold.

In principle, Eqs. (1) extend from $E = 0 \rightarrow \infty$ since a filtered array generates *some* data for all x-ray photons; but practically there is a *finite* spectral domain $[E_{min}, E_{max}]$ over which the array almost exclusively responds for a given experiment. The *a priori* information needed to make this determination may come from so-called background or null experiments, plasma theory, or simulations. For the response functions of Fig. 1 and Z-pinch experiments, the photon energy E_{min} is identified with 137 eV because all the R_i's are $\leq$~1% of their peak values below this photon energy. It is assumed, therefore, that f is not dominated by intense XUV at lower energies. Similarly, one may argue that at the Z facility the emission and detection of x rays in the keV energy range are relatively less likely than of softer photons thermalized in the Z-pinch plasma. If one selects $E_{max} \approx 2300$ eV, then even blackbody spectra of temperatures ~250 eV have integrated flux levels of only a few per cent in photons of energy $> E_{max}$.

The partition of the spectral domain is then defined to make the matrix $\boldsymbol{R}$ as close to diagonal as possible while still allowing some flexibility in the unfold from anticipated spectra. The easily-distinguished, K- and L-edge features in response functions R_1, R_2, and R_3 (Fig. 1) suggest joints at photon energies 284, 513, and 1020, eV (Figs. 10-11); the low energy portions of these responses (*i.e.*, excluding the "hump") are nearly non-overlapping. The additional joint at 1500 eV was added after a series of simulations with blackbody spectra.

Appendix II. Properties of averaging kernels

The purpose of this appendix is to describe heuristically some of the integral properties of AK's that relate to the Backus Gilbert method — in particular, to motivate the constraint Eq. (4) and the use of A_{BG}^2 in Eq. (3). The inaccuracy between f_{BG} and f is also considered. It should be noted that AK's can be constructed from other criteria than the BG method[14-16].

The estimate f_{BG} in Eq. (7) depends on the fixed source function f and a function $A(E_0, E)$, which is constructed for each photon energy E_0 chosen. The result of integrating these two factors $\int f(E)A(E_0, E)dE$ is a *function* of E_0 and a *functional* of f. Simple and convenient forms of A are often studied. For example, A may be non-negative with a local maximum at $E = E_0$. Or, A may depend only on the difference $(E_0 - E)$, thus retaining its shape for all E_0 and reducing the integral to a convolution. But, in general, the E_0 and $A(E_0, E)$ may be related in a very complicated way: that is, $A(E_0, E)$ may (a) change its shape for different choices of E_0, (b) be positive- or negative-valued or zero within its domain, (3) be asymmetric about E_0, and (d) be peaked elsewhere than E_0. (See Fig. 6). In the BG formalism the mathematical diagnostics of width and center are aimed at characterizing such behavior.

What properties of the AK $A_{BG}(E_0, E)$ in Eq. (7) make $f_{BG}(E_0)$ at least *approximately*

equal to $f(E_0)$? Clearly, if $A(E_0,E) = \delta(E - E_0)$, the Dirac δ function, the problem would be trivial. But for most physical problems A_{BG} has finite width. Since the AK in the Backus-Gilbert analysis is specified as a linear combination of the given response functions [Eq. (2)], a more appropriate question is this: if one were to chose among a *collection* of AK's A_λ, all defined at E_0 and applied to Eq. (7), which would produce the most accurate estimate of $f(E_0)$?

To explore this point, consider first the special case in which $A(E_0,E)$ is non-negative and symmetric about E_0. Also assume that $f(E)$ is slowly varying over the width of $A(E_0,E)$ and expanded in a Taylor series about fixed E_0. Then, $\int f(E)A(E_0,E)dE$ becomes

$$\int f(E)A(E_0,E)dE = f(E_0)\int A(E_0,E)dE + f'(E_0)\int A(E_0,E)(E - E_0)dE +$$

$$\frac{1}{2}f''(E_0)\int A(E_0,E)(E - E_0)^2 dE + \ldots \equiv f_{BG}(E_0) \quad (12),$$

where the symbols (′) and (″) denote single and double differentiation, respectively. The integrals in the middle of Eq. (12) can be regarded as moments of A about E_0. Suppose now that the function $A(E_0,E)$ is normalized by dividing through with the zeroth-order moment $\int A(E_0,E)dE$; *i.e.*, constraint Eq. (4) is adopted. Then, remembering that $A(E_0,E)$ is assumed symmetric about E_0, one finds $f_{BG}(E_0) \approx f(E_0)$ with a second-order correction proportional to $f''(E_0)$ plus higher order corrections proportional to even-order derivatives of f at E_0. Thus, in choosing among a *collection* of so-normalized functions A_λ to achieve the *best* local approximation to $f(E_0)$, one might then chose the A_λ which minimizes $\int A_\lambda(E_0,E)\,(E - E_0)^2\,dE$. The narrower $A(E_0,E)$, the smaller is the correction. Of course, one might choose other "narrowness" criteria; in particular, the BG method chooses to minimize $\int A_\lambda(E_0,E)^2\,(E - E_0)^2 dE$, Eq. (3).

When the AK A is not required to be symmetric about E_0 or non-negative, it is usually still possible to normalize A with the zeroth moment, but the estimate of $[f_{BG}(E_0) - f(E_0)]$ is more complicated. It is then convenient to decompose A into symmetric and antisymmetric components[33] about E_0: $A(E_0,E) = A_{even}(E_0,E) + A_{odd}(E_0,E)$. Again forming $\int A(E_0,E)f(E)dE$ and expanding f about E_0, one obtains the same type of terms as in Eq. (12), except that now the first- and second-order correction terms become, respectively, $f'(E_0)\int A_{odd}(E_0,E)(E - E_0)dE$ and $\frac{1}{2}f''(E_0)\int A_{even}(E_0,E)(E - E_0)^2 dE$. As above, if one were sorting through a collection of AK's A_λ to get the closest approximation or local average to $f(E_0)$, one would now need to choose *both* A_{even} and A_{odd} as narrow as possible. Here the BG criterion Eq. (3) becomes really useful: since $\int A_\lambda^2(E - E_0)^2\,dE = \int[A_{odd}^2 + A_{even}^2](E - E_0)^2\,dE$, selecting $\int A_\lambda^2(E - E_0)^2\,dE$ small restricts both even and odd components of A.

The terms in the series of Eq. (12) divide the discrepancy between f_{BG} and f into two independent parts: moments of the AK (related to the width) and derivatives of the source function f (related to its local shape). One can then qualitatively understand the behavior of

f_{BG} relative to f in Figs. 4 and 10 by examining these terms. A dependence on f'' is particularly clear: *e.g.,* where f'' is small (in the nearly linear sections), f_{BG} approximates f fairly well; but where f'' is large (*e.g.,* at the peak and in the exponential tail region), f_{BG} is less accurate. The sign of $f_{BG} - f$ also follows f''. That the effect of f' in this example is small can be seen in Fig. 11, which is like Fig. 10, except the simulating source function has been constructed with a straight section at high photon energies. In this region, the second derivative of f is zero, and f_{BG} at the points of best resolution approximates f more closely than in Fig. 10.

Sandia is a multiprogram laboratory operated by Sandia Corporation, a Lockheed Martin Company, for the United States Department of Energy under contract DE-AC04-94AL85000.

REFERENCES:

1. N. A. Dyson, *X rays in Atomic and Nuclear Physics,* 2nd Ed. (Cambridge University Press, NY: 1990).
2. T. F. Stratton, "X-ray Spectroscopy," in *Plasma Diagnostic Techniques*, R. H. Huddlestone and S. L. Leonard, eds., (Academic Press, NY: 1965).
3. G. A. Chandler, *et. al.*, Rev. Sci. Instrum. **63**, 4828 (1992).
4. H. N. Kornblum, R. L. Kauffman, and J. A. Smith, Rev. Sci. Instrum. **57**, 2179 (1986).
5. J. F. Cuderman and K. M. Glibert, Rev. Sci. Instrum. **46(1),** 53 (1975).
6. G. C. Idzorek and R. J. Bartlett, "Silicon Photodiode characterization from 1 eV to 10 keV," in "EUV, X-ray and Gamma-Ray Instrumentation for Astronomy VIII, O. H. W. Sigmund, M. A. Gummin, eds., *Proceedings of the SPIE* **3114** 349 (1997).
7. R. B. Spielman, Rev. Sci. Instrum., **63(10)** 5056 (1992).
8. K. L. Baker, *et. al.*, Rev. Sci. Instrum., **70(4)** 2012 (1999).
9. G. A. Chandler, *et. al.*, Rev. Sci. Instrum. **70(1)**, 561 (1999).
10. R. B. Spielman, *et. al.*, Phys. Plasmas **5**, 2105 (1998).
11. R. B. Spielman, *et. al.*, Rev. Sci. Instrum. **70(1)**, 651 (1999).
12. D. L. Fehl, *et. al.*, Rev. Sci. Instrum. **70(1)**, part II, 270 (1999).
13. J. L. Porter, Sandia National Laboratories, private communication.
14. M. Bertero, "Linear Inverse and Ill-posed Problems," in *Advances in Electronics and Electron Physics* (ed. P. W. Hawkes) vol 75 (Academic Press, London: 1989) p 1.
15. M. Bertero, C. De Mol, and E. R. Pike, Inverse Problems **1**, 301 (1985).
16. M. Bertero, C. De Mol, and E. R. Pike, Inverse Problems **4**, 573 (1988).
17. M. Bertero and P. Boccacci, *Introduction to Inverse Problems in Imaging* (Institute of Physics Publishing, Philadelphia: 1998).
18. V. B. Glasko, *Inverse Problems of Mathematical Physics*, (American Institute of Physics, New York:1984).
19. I. J. D. Craig and J. C. Brown, *Inverse Problems in Astronomy*, (Adam Hilger, Boston:

1986).

20. S. Twomey, *Introduction to the Mathematics of Inversion in Remote Sensing and Indirect Measurements*, (Dover Publications, Mineola, New York: 1996).

21. A. N. Tikhonov and V. Y. Arsenin, *Solutions of Ill-posed Problems*, (John Wiley, New York: 1977).

22. G. E. Backus and J. F. Gilbert, Geophys. J. R. Astr. Soc. **13**, 247 (1967).

23. G. E. Backus and J. F. Gilbert, Geophys. J. R. Astr. Soc. **16**, 169 (1968).

24. G. E. Backus and J. F. Gilbert, Phil. Trans. R. Soc. **266**, 123 (1970).

25. Not all combinations are improvements: *e.g.,* forming a linear combination of R_1 and R_2 generates a wider response than either of the components.

26. L. Kissel, F. Biggs, and T. Marking, "UFO (Unfold Operator): USER GUIDE: PART I – Overview and Brief Command Descriptions," Sandia National Laboratories Report SAND82-0396 UC-705 (Sandia National Laboratories, Albuquerque, NM, June 1991), unpublished.

27. The numerical factor of 12 in Eq. (6) was inserted by Backus and Gilbert so that the spread of a single histogram $B(E)$, defined as $B = 1/\ell$ for $|E - E_0| \leq \ell/2$ (0 otherwise), is ℓ about its center $c = E_0$. Apart from this factor, one also sees that Eq. (3) represents a minimization of the width of A_{BG} about fixed E_0 as the scalars α_i are varied subject to the constraint Eq. (4).

28. In the simple example of Fig. 3, the "modified" response functions were not re-normalized in the sense of Eq. (4).

29. T. W. L. Sanford, *et. al.*, Rev. Sci. Instrum. **68**, 852 (1997).

30. D. L. Fehl, R. J. Leeper, and R. P. Kensek, Rev. Sci. Instrum. **63(10)**, 4786 (1992).

31. G. E. Forsythe, M. A. Malcolm, and C. B. Moler, *Computer methods for mathematical computations*, (Prentice-Hall, Englewood Cliffs, N. J.:1977).

32. W. H. Press, *et. al., Numerical recipes in FORTRAN: The art of scientific computing*, (Cambridge University Press, NY: 1992).

33. The properties of these functions are $A_{even}(E_0, E-E_0) = A_{even}(E_0, E_0-E)$ and $A_{odd}(E_0, E-E_0) = -A_{odd}(E_0, E_0-E)$. Explicitly, $A_{even} = \frac{1}{2}[\, A(E_0, E) + A(E_0, 2E_0 - E)]$ and $A_{odd} = \frac{1}{2}[\, A(E_0, E) - A(E_0, 2E_0 - E)]$.

FIGURE CAPTIONS:

1. Five response functions for a filtered-XRD array, fielded at the Z facility on line-of-sight (LOS) 5/6. The sharp features at low energies are due to the x-ray absorption edges of filters, photocathodes, and surface contaminants. A "hump" feature appears at higher energies as the filters become transparent to x-ray photons, and photo absorption in the photocathode dominates the overall spectral response. All the response functions are ≤~1% of peak values for $E \leq E_{min} = 137$ eV.

2. Time-dependent, filtered-XRD voltage traces for shot Z-306, LOS 5/6. The set of signals {XRDi} correspond to the calibrated response functions $\{R_i\}$ used in this shot, which are similar to those in Fig. 1. The voltage traces must be multiplied by known geometric and electrical factors to obtain time-dependent data $g_i(t)$ in units consistent with Eq. (1). See Ref. 9 and Fig. 5.

3. Example of the Backus-Gilbert approach. (a) A hypothetical set $\{R_1,R_2,R_3\}$ of simple response functions: $R_1(E) = h_1$ for $|E - E_1| < \Delta E$ (0 otherwise); $R_2(E) = h_2$ for $|E - E_3| < \Delta E$ (0 otherwise); and $R_3(E) = h_3$ for $|E - E_4| < 2\Delta E$ (0 otherwise), where $E_j = E_1 + (j - 1)\Delta E$, ($j = 1,2, \ldots ,5$). (b) A modified set of response functions $\{R_1,R_2, R_3'\}$is formed as a linear combination of $\{R_1,R_2,R_3\}$. The modified responses are not normalized in the sense of Eq. (4).

4. Comparison of a test source function f (150 eV blackbody spectrum) and the continuous Backus-Gilbert approximating function f_{BG}, constructed from data which were simulated from f folded with the response functions of Fig. 1. There are no adjustable parameters.

5. Data simulated from test spectra and the response functions of Fig. 1. The solid circles in the lower curve refer to the 150 eV blackbody spectrum of Fig. 4; the diamond symbols refer to the spectrum of Fig. 11. The line segments between symbols in both curves are shown to guide the eye. The units of these data come from the spectrum (W/sr-cm^2-eV), the response functions (A/MW), and Eqs. (1) with photon energy in eV.

6. The Backus-Gilbert averaging kernel $A_{BG}(E_0 ,E)$ at selected energies of interest $E_0 = 250$, 350, 450, and 600 eV. These functions are here displaced along the ordinate axis for clarity, but the relative size has been preserved. The center $c(E_0)$ is noted for each curve with a dotted vertical line. Since A_{BG} is constructed as a linear combination of the XRD response functions, x-ray absorption features of these underlying functions can still be recognized.

7. Backus-Gilbert width function w for A_{BG} as a function of E_0. The arrows indicate the values of E_0 for which A_{BG} is shown in Fig. 6.

8. Backus-Gilbert center function c for A_{BG} as a function of E_0. The arrows indicate the values of E_0 for which A_{BG} is shown in Fig. 6 Where $c(E_0)$ crosses the dotted diagonal line the point of interest and center coincide (*e.g.*, at E_0 = 250, 450 eV, ...).

9. The five "narrowest" BG averaging kernels, defined by local minima in Fig. 7, to be compared with the original response functions in Fig. 1.

10. Comparison of the test source function f (a 150 eV blackbody) with selected points of the BG approximating function f_{BG} and a histogram unfold of Eq. (1), both from simulated data. The BG reconstruction corresponds to the narrowest averaging kernels shown in Fig. 9; these points are included, but not specifically noted, in Fig. 4. The horizontal bars represent the BG width of the AK's and are interpreted as the resolution available from the given response functions. The bins and domain (137 - 2300 eV) for the standard unfold are discussed in Appendix I and were obtained independently of the BG resolution.

11. Test of Eq. (12) in Appendix II. A comparison of a modified test source function f (solid line) with selected points of the BG approximating function f_{BG} and a histogram unfold from simulated data. The tail of the 150 eV blackbody spectrum (Figs. 4 and 10) has been replaced by a linear segment to eliminate second-derivative effects in the source at high energies. The horizontal bars are the same resolution bands as in Fig. 10.

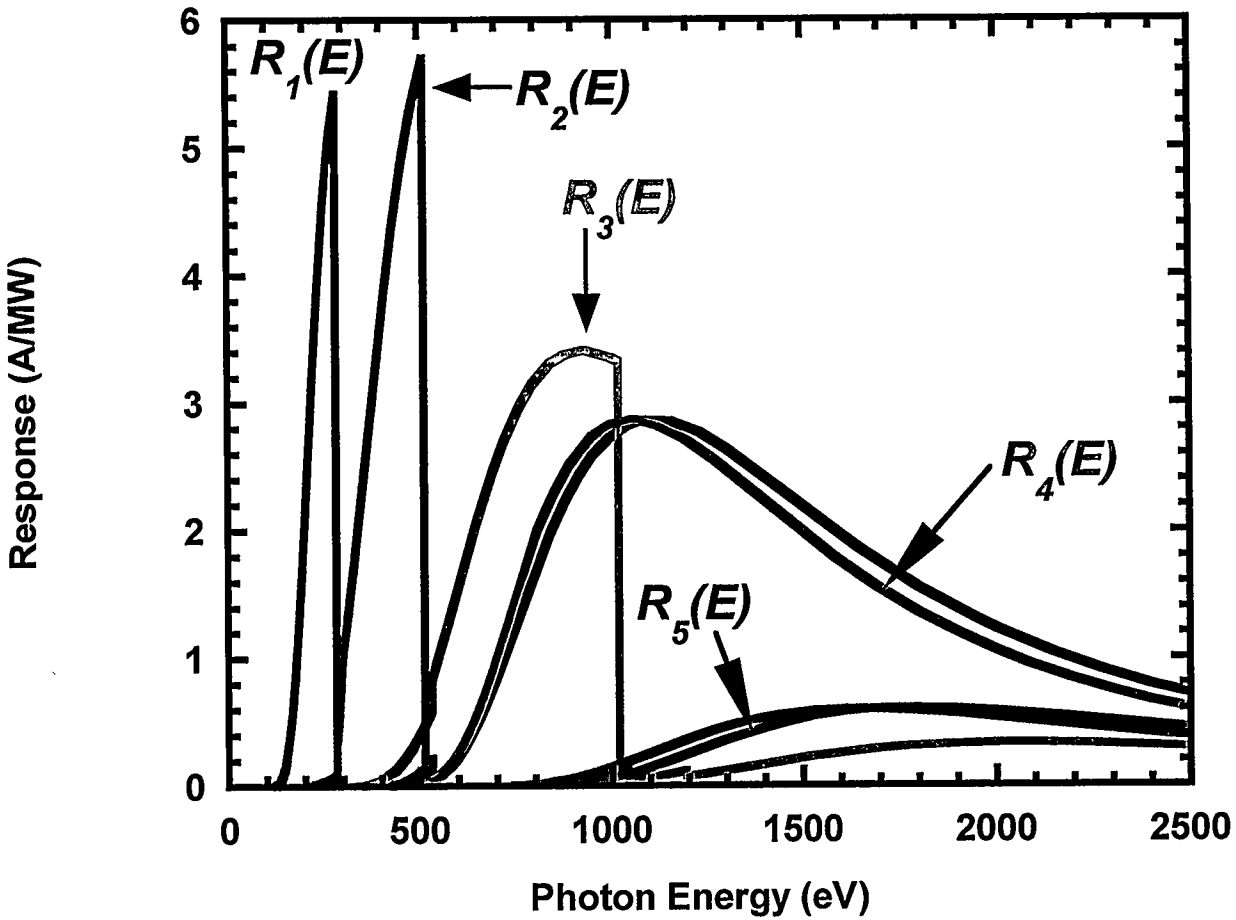
Response (A/MW)
Photon Energy (eV)
$R_1(E)$
$R_2(E)$
$R_3(E)$
$R_4(E)$
$R_5(E)$
0
1
2
3
4
5
6
0
500
1000
1500
2000
2500

Fig 1

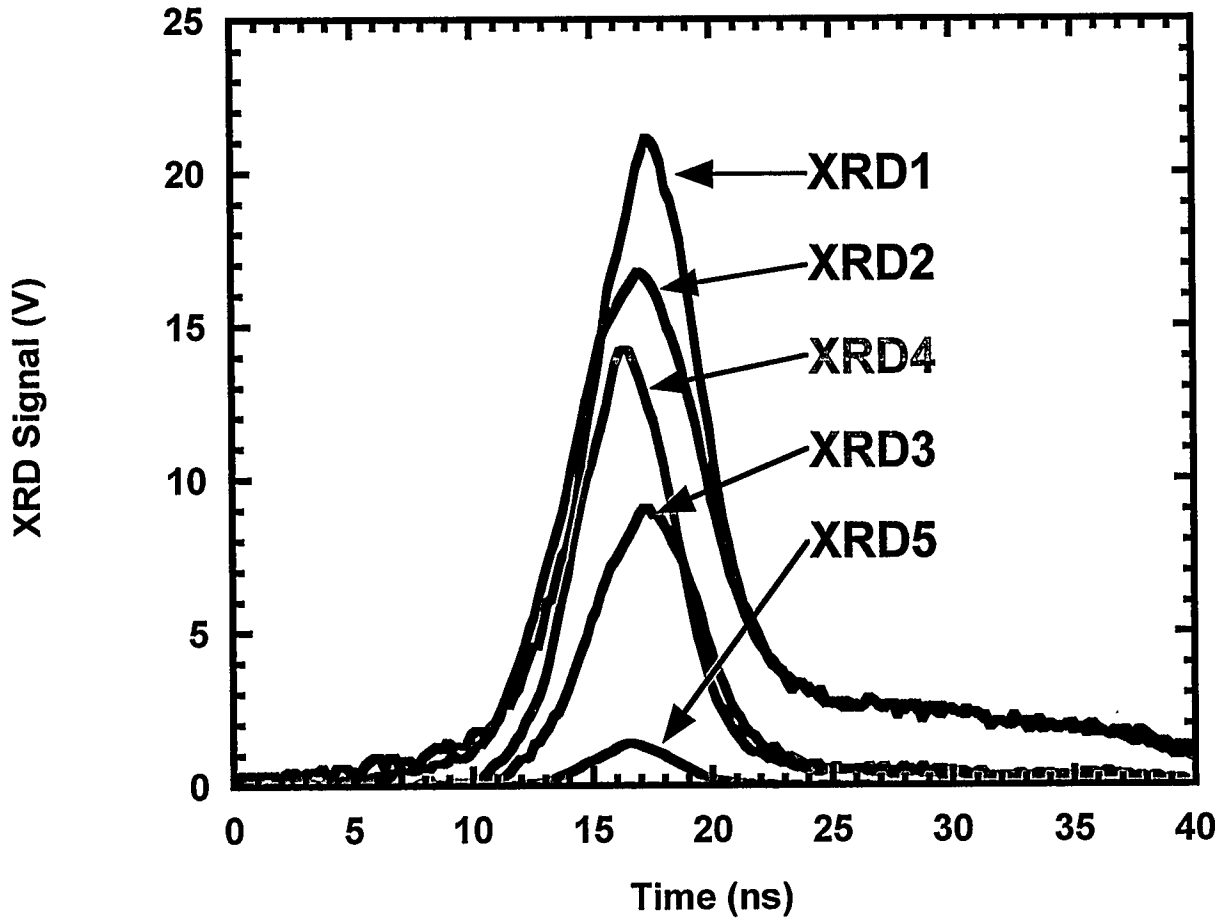
XRD Signal (V)
25
20
15
10
5
0
0
5
10
15
20
25
30
35
40
Time (ns)
XRD1
XRD2
XRD4
XRD3
XRD5

Fig 2

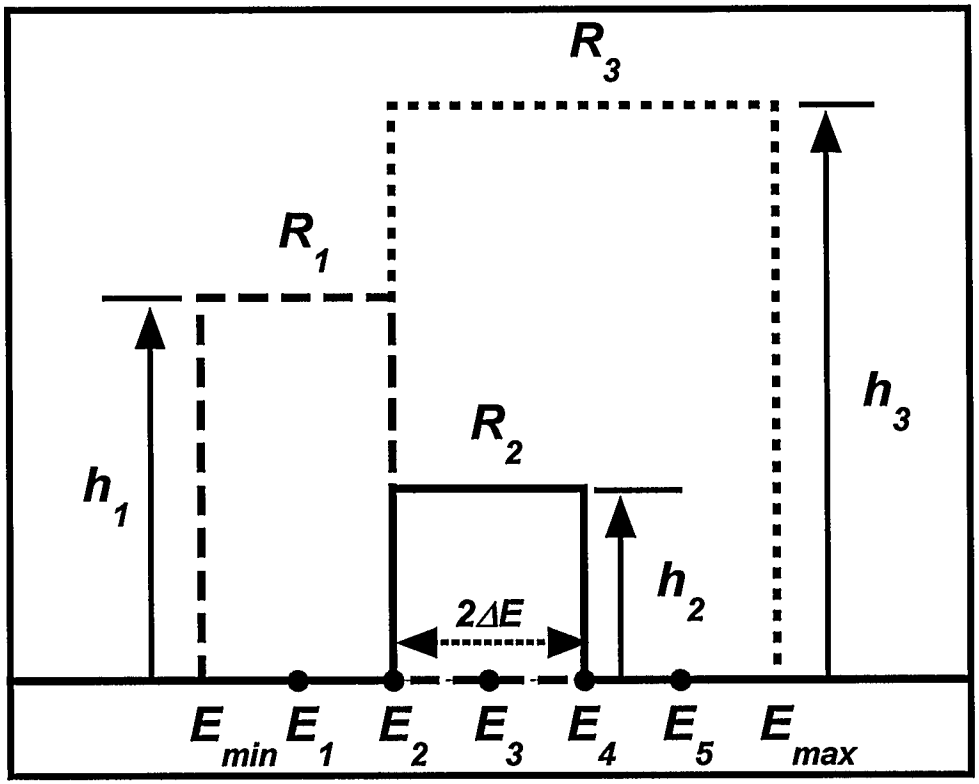

Fig 3a

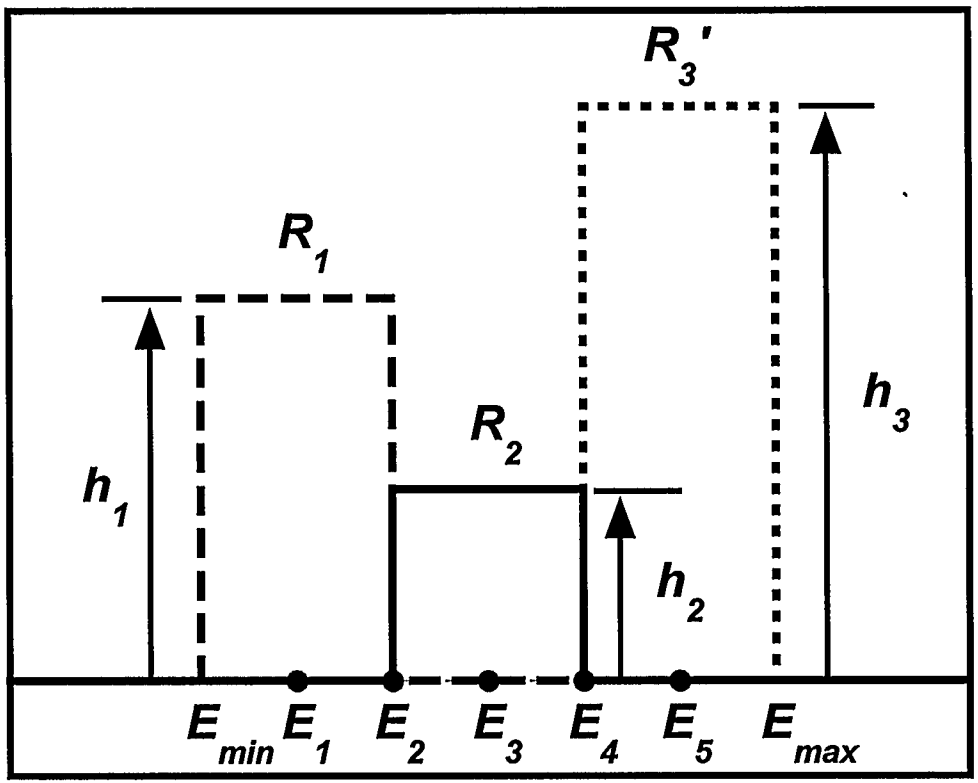

Fig 3b

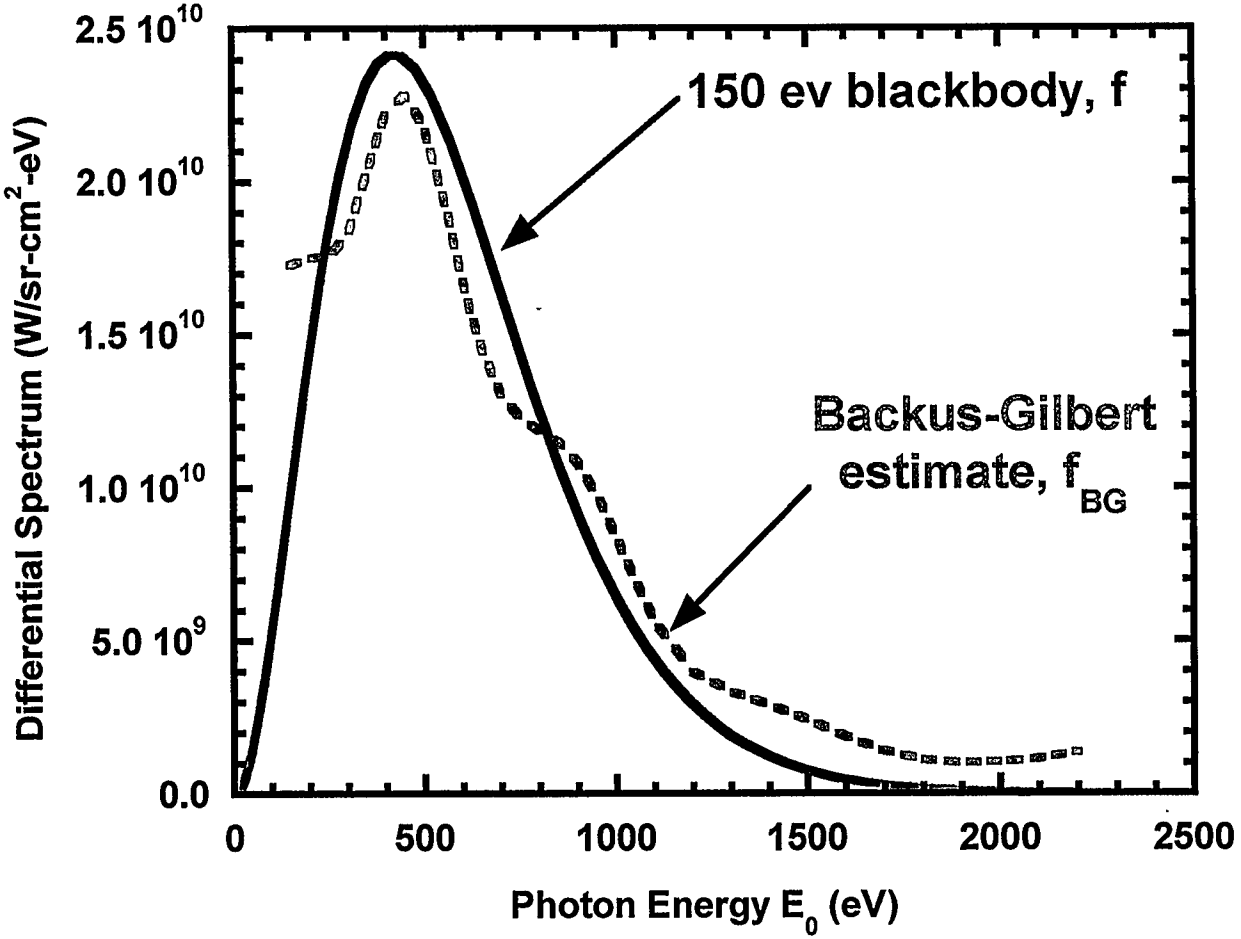
2.5 10^10
2.0 10^10
1.5 10^10
1.0 10^10
5.0 10^9
0.0
Differential Spectrum (W/sr-cm^2-eV)
150 ev blackbody, f
Backus-Gilbert
estimate, f_BG
0
500
1000
1500
2000
2500
Photon Energy E_0 (eV)

Fig 4

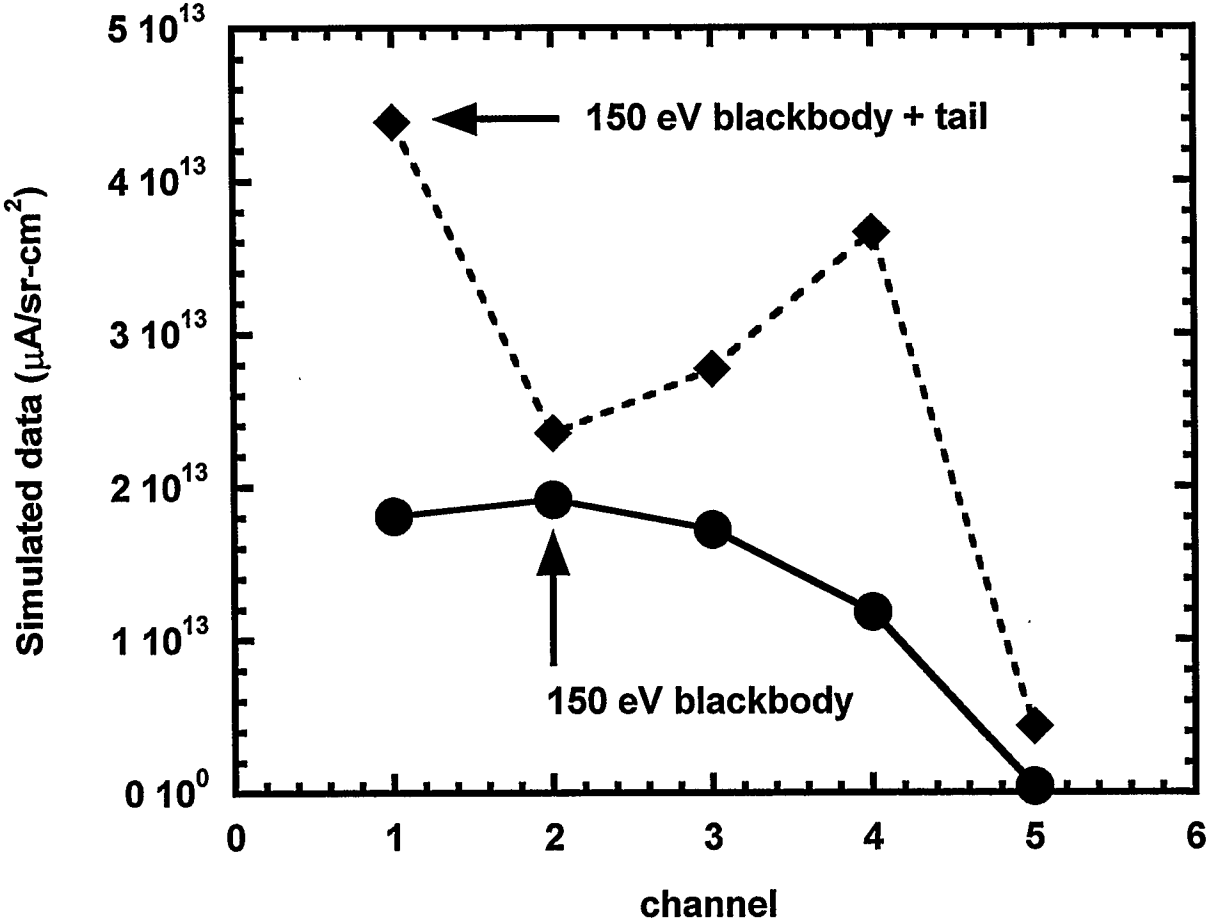
5 10^13
4 10^13
3 10^13
2 10^13
1 10^13
0 10^0
Simulated data (μA/sr-cm^2)
150 eV blackbody + tail
150 eV blackbody
0
1
2
3
4
5
6
channel

Fig 5

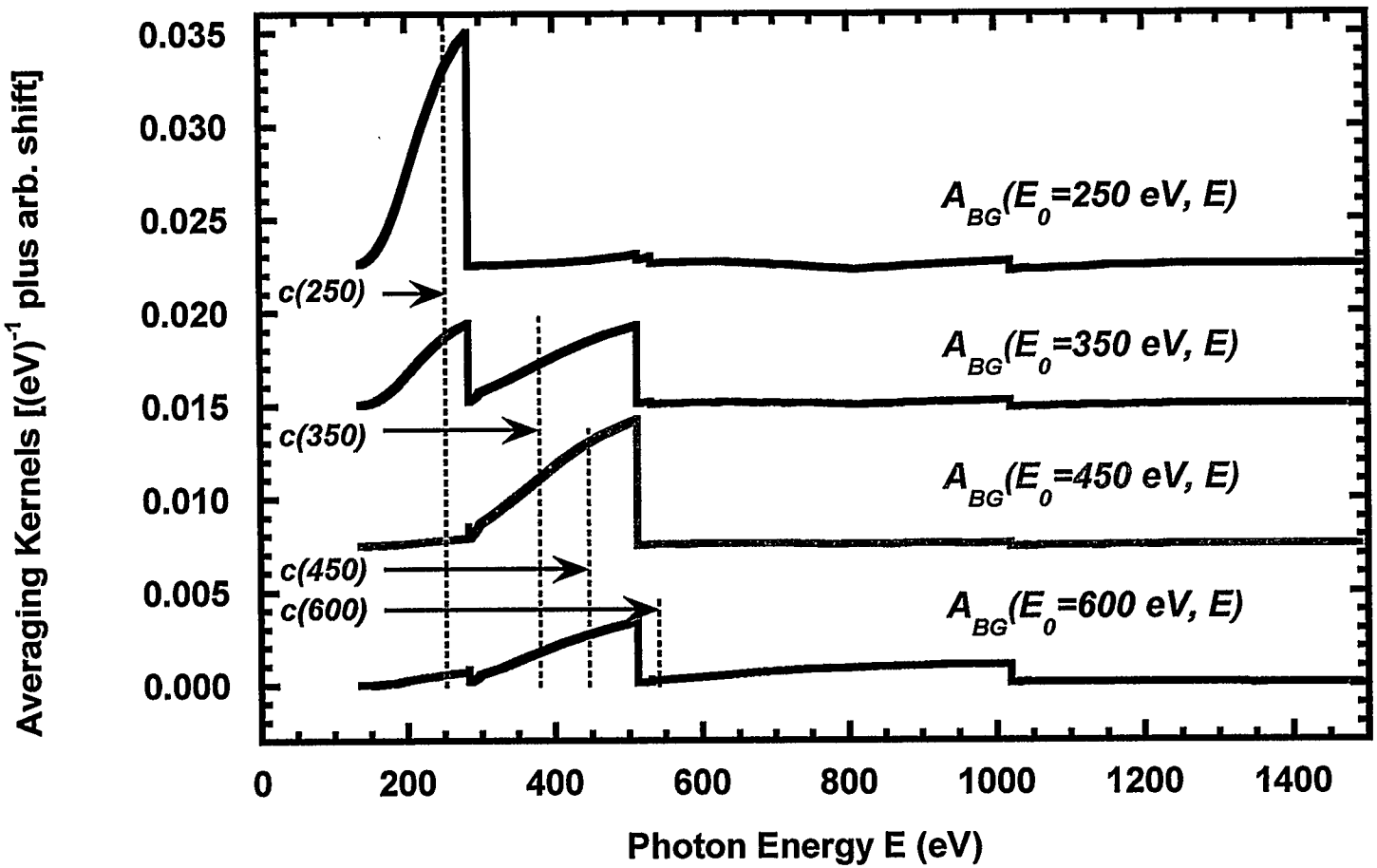
Averaging Kernels [(eV)$^{-1}$ plus arb. shift]
0.035
0.030
0.025
0.020
0.015
0.010
0.005
0.000
$A_{BG}(E_0$=250 eV, E)
$A_{BG}(E_0$=350 eV, E)
$A_{BG}(E_0$=450 eV, E)
$A_{BG}(E_0$=600 eV, E)
c(250)
c(350)
c(450)
c(600)
0
200
400
600
800
1000
1200
1400
Photon Energy E (eV)

Fig 6

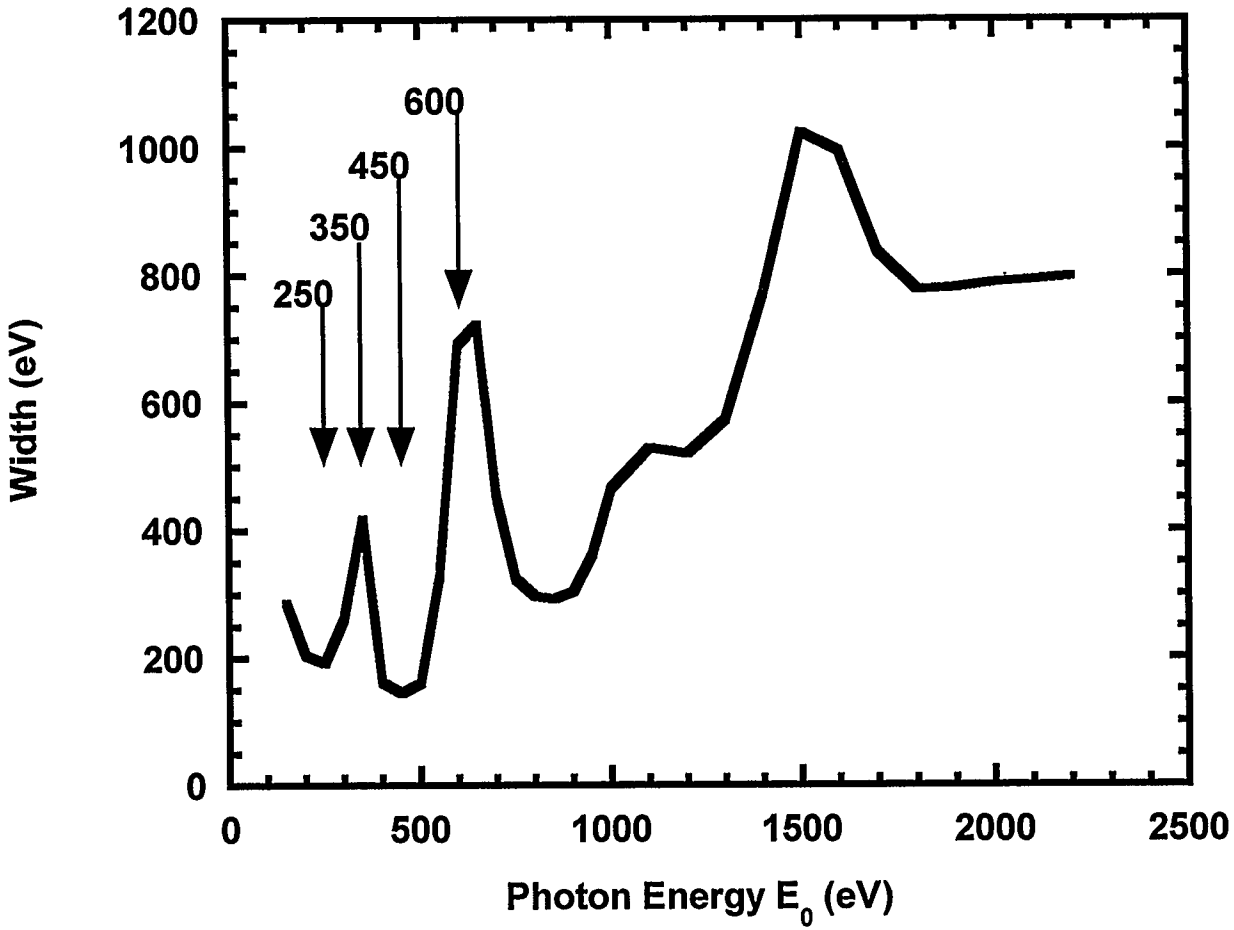
1200
1000
800
600
400
200
0
Width (eV)
600
450
350
250
0
500
1000
1500
2000
2500
Photon Energy E0 (eV)

Fig 7

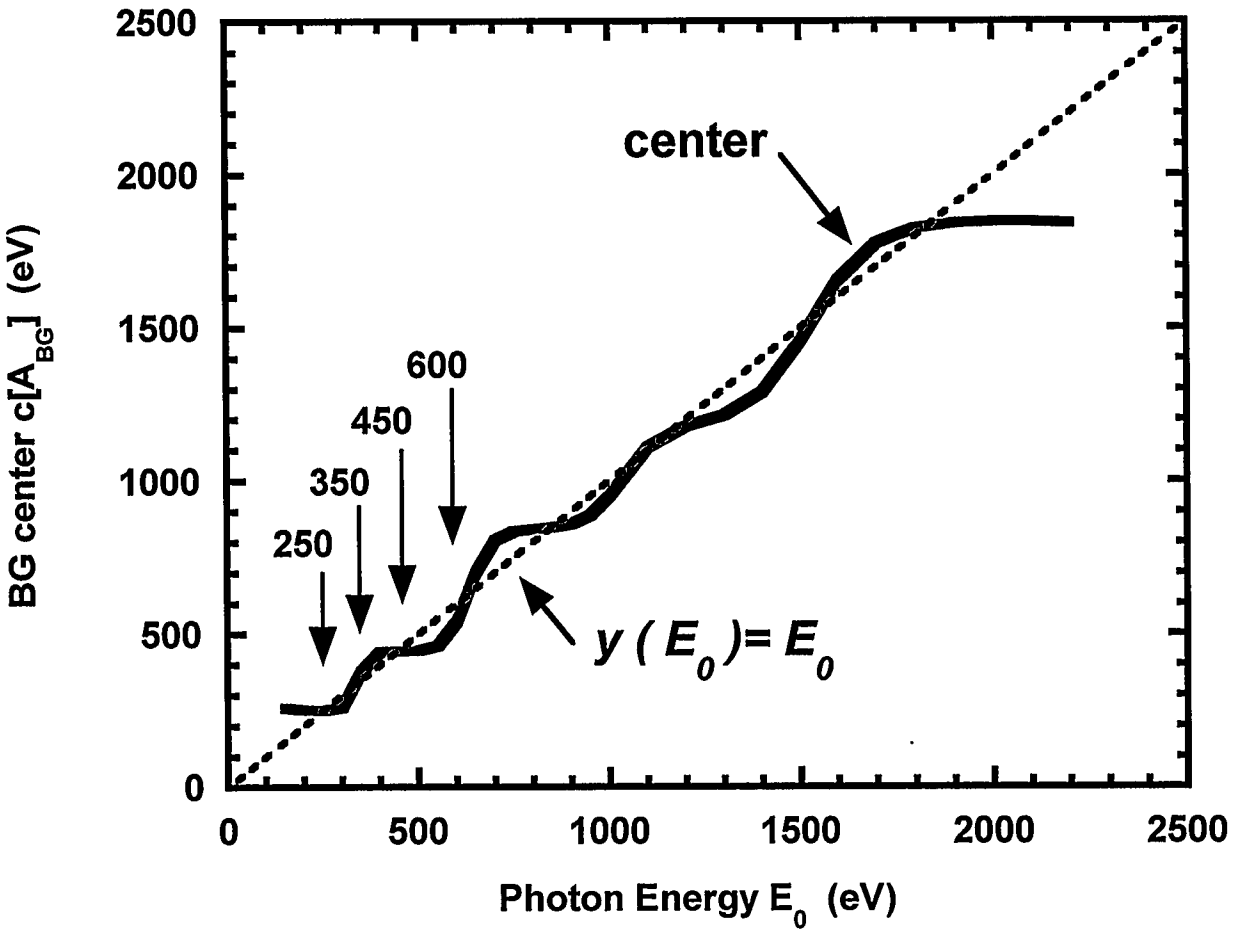
2500
2000
1500
1000
500
0
0
500
1000
1500
2000
2500
BG center c[A_BG] (eV)
Photon Energy E_0 (eV)
center
600
450
350
250
y (E_0)= E_0

Fig 8

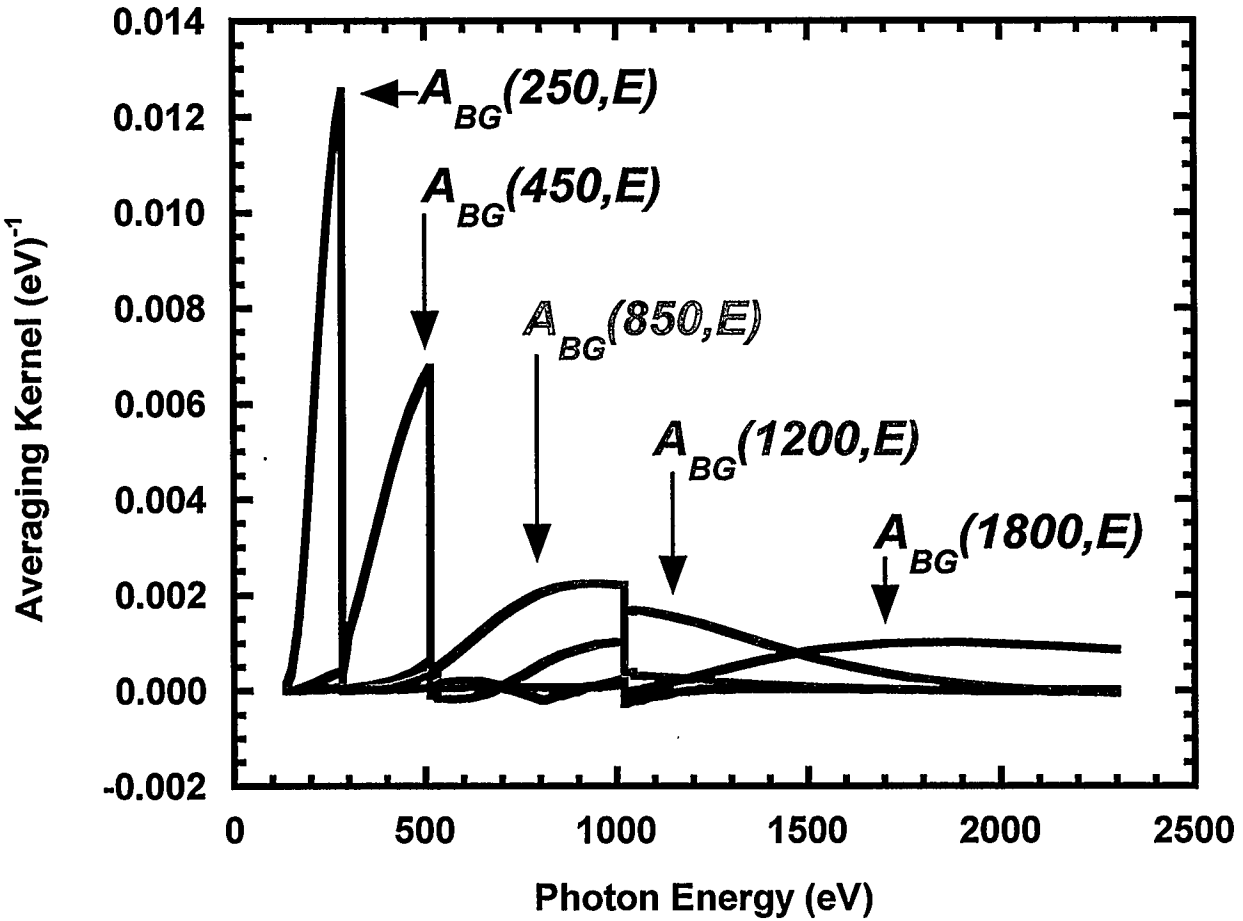
0.014
0.012
0.010
0.008
0.006
0.004
0.002
0.000
-0.002
Averaging Kernel (eV)-1
A BG(250,E)
A BG(450,E)
A BG(850,E)
A BG(1200,E)
A BG(1800,E)
0
500
1000
1500
2000
2500
Photon Energy (eV)

Fig. 9

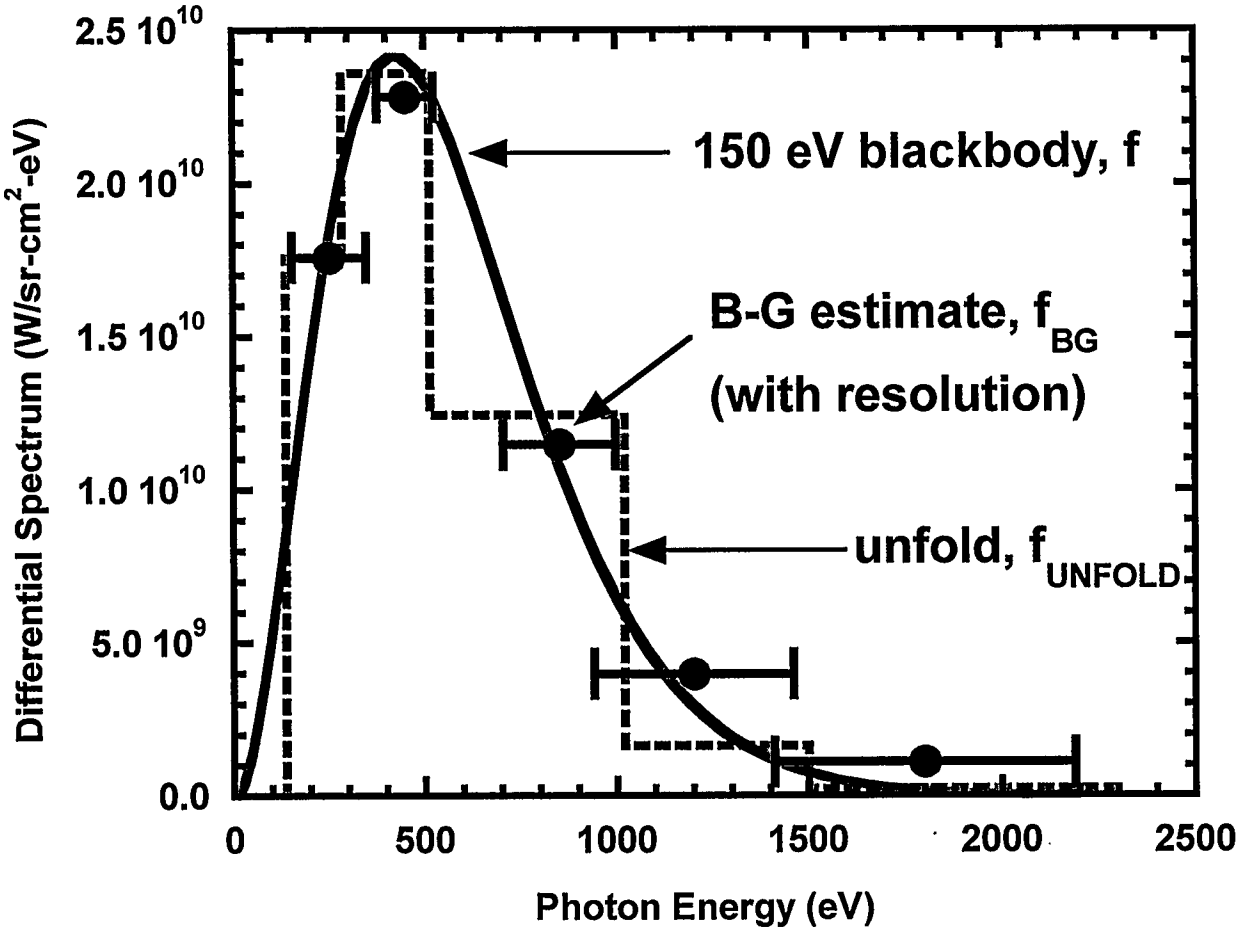
2.5 10^10
2.0 10^10
1.5 10^10
1.0 10^10
5.0 10^9
0.0
Differential Spectrum (W/sr-cm^2-eV)
0
500
1000
1500
2000
2500
Photon Energy (eV)
150 eV blackbody, f
B-G estimate, f_BG
(with resolution)
unfold, f_UNFOLD

Fig 10

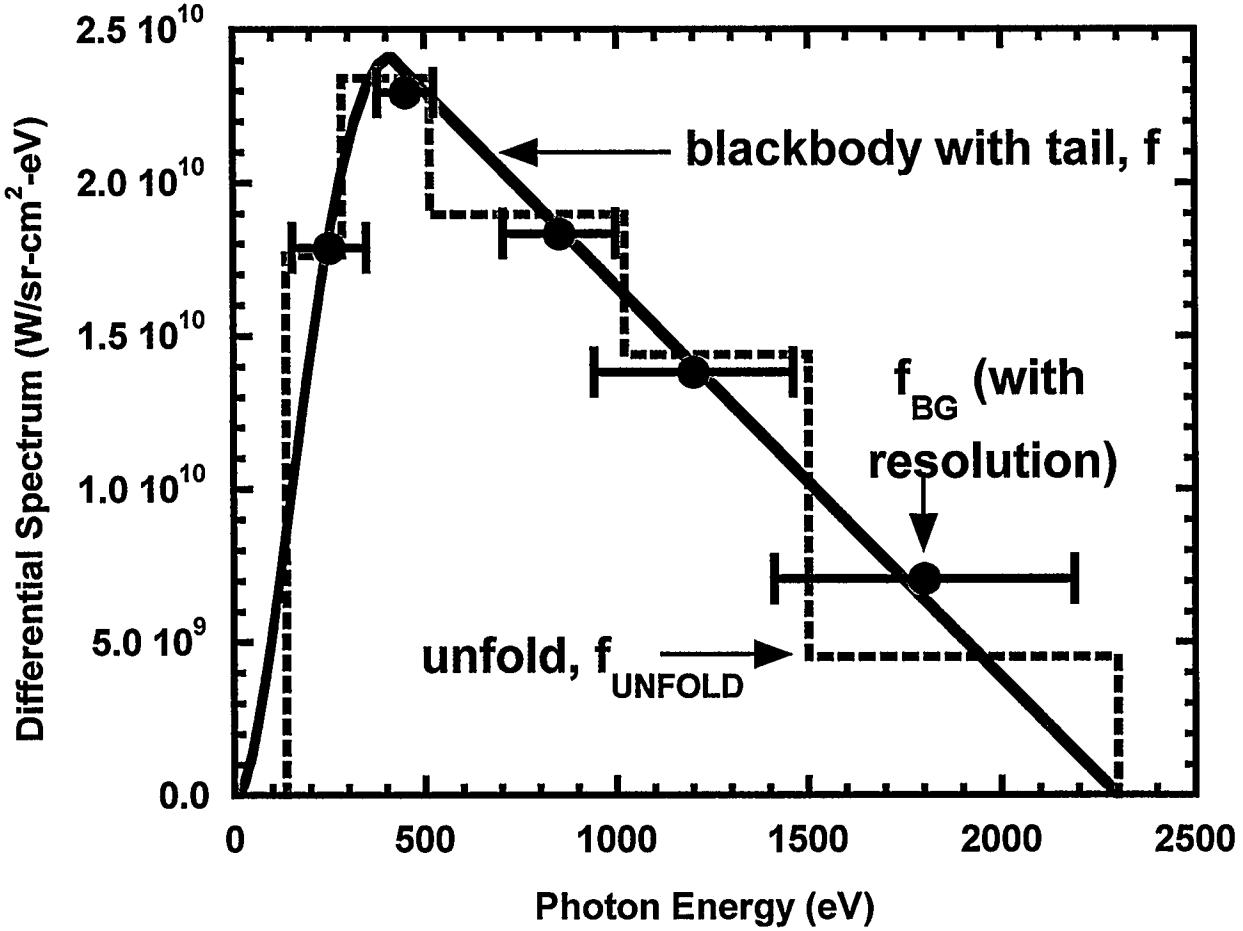
2.5 10^10
2.0 10^10
1.5 10^10
1.0 10^10
5.0 10^9
0.0
Differential Spectrum (W/sr-cm^2-eV)
0
500
1000
1500
2000
2500
Photon Energy (eV)
blackbody with tail, f
f_BG (with resolution)
unfold, f_UNFOLD

Fig 11